IV International Conference on Particle-based Methods – Fundamentals and Applications
PARTICLES 2015
E. Oñate, M. Bischoff, D.R.J. Owen, P. Wriggers & T. Zohdi (Eds)

AN INVESTIGATION INTO THE EFFECT OF PARTICLE PLATYNESS ON THE STRENGTH OF GRANULAR MATERIALS USING THE DISCRETE ELEMENT METHOD

M. POTTICARY[1], A. ZERVOS[1] AND J. HARKNESS[1]

[1] Infrastructure Research Group, Faculty of Engineering and the Environment, University of Southampton
University Rd, Southampton, SO17 1BJ
M.Potticary@soton.ac.uk

Key words: Granular Materials, DEM, Contact Problems, Ballast

Abstract. It has long been recognised that the macroscopic mechanical behaviour of a granular material depends, to differing extents, on micro-mechanical properties such as the particle size distribution, the particle shape, the inter-particle friction angle and the particle strength. However, a systematic investigation of some of these effects is still lacking. In this paper we focus on particle shape, which is one of the fundamental characteristics of a granular material.

We build on previous work that used the axes of an equivalent scalene ellipsoid to characterise particle form, one of the three aspects that define particle shape. (The other two being angularity and roughness.) We use DEM simulations to investigate the effect of particle form, and in particular of particle platyness, on the friction angle of a granular material at critical state. It is found that a deviation of particle shape from that of a sphere leads to higher angles of friction; quantities such as fabric, average rates of particle rotation and interparticle sliding are used to provide insights into the underlying micromechanics.

1 Introduction

The shape of its particles is one of the fundamental properties of a granular material. To quantify it, three (assumed) independent aspects of shape are generally considered, each describing geometrical properties of a particle at a different scale of observation. These are particle form, angularity and roughness. Form quantifies the overall shape of a particle, angularity describes the number and sharpness of angles on its perimeter/surface, and roughness relates to the microscopic variations of the particle surface that are to some extent responsible for interparticle friction.

Particle form in particular is generally quantified using the longest (L), intermediate (I) and shortest (S) dimensions of the particle. Whilst a number of different measures

have been proposed to describe form, generally involving combinations of S, I and L, no consensus exists on whether one has a clear advantage over the others [8].

Here we propose a new way of describing form on the basis of an equivalent scalene ellipsoid with axes equal to the dimensions S, I and L of the particle. In this framework, particle form is uniquely defined by two parameters: particle *elongation* and *platyness*. We then perform DEM simulations of triaxial compression on granular assemblies of the same particle size distribution, each consisting of particles of a single form, to investigate the effect of particle platyness. We use the method of potential particles, which allows modelling of particles with (almost) arbitrary shape. Particle size distributions consistent with those of railway ballast are used, while the number of particles in each simulation is consistent with the number of ballast particles present in the specimens of corresponding physical tests.

2 Particle Form

Over the years many different ways to describe particle form have been presented, with many authors contributing to the debate [2, 13, 7, 27, 26, 25, 24, 23, 17, 16]. One of the most common methods is to use a simple solid to represent the particle, and assume that the form of the particle can be determined with reference to the geometry of that solid. The simplest such solid that can be defined in 3D is a sphere.

The definition of form that we use in this study is detailed in [20]. A scalene ellipsoid is used as reference solid; such an ellipsoid is the simplest smooth shape that allows three independent radii, corresponding to a particle's longest (L), intermediate (I) and shortest (S) dimensions. If we consider S , I and L to be coordinates in a three dimensional space, any particle can be represented by a vector $\mathbf{f}$ linking the origin of the axes to point (S, I, L). Clearly the shape (form) of the particle is represented by the orientation of $\mathbf{f}$, whereas the length of $\mathbf{f}$ merely quantifies the size of the particle.

To quantify form we consider the intersection F of $\mathbf{f}$ with the $S + I + L - 1 = 0$ "deviatoric" plane, which is normal to the spherical axis $S = I = L$ along which all spherical particles plot. The form of each particle is then uniquely defined by the two in-plane coordinates of F in a frame of reference centered at the intersection P of the spherical axis. In this way particle form is essentially quantified as the deviation of a particle's shape from that of a sphere. These two independent parameters of form, normalised in the $[0, 1]$ interval for ease of use, are given by Equations 1 and are referred to as *platyness* (α) and *elongation* (ζ) respectively.

$$\alpha = \frac{2(I - S)}{L + I + S}, \qquad \zeta = \frac{L - I}{L + I + S} \tag{1}$$

Ellipsoids that share the same values for both α and ζ are geometrically similar, i.e. they differ only in size but not shape. All possible scalene ellipsoids plot, on the α-ζ plane, within the triangle shown in Figure 1. The edges and corners of the triangle correspond to degenerate cases where some of the dimensions are equal and/or zero.

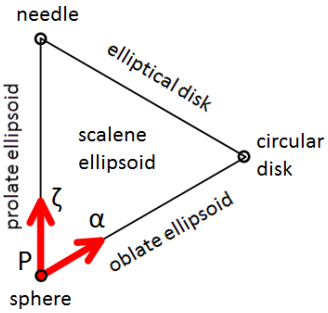

Figure 1: Elongation and Platyness space with description of forms

In [22, 21, 12, 11, 9, 5, 4, 3, 18] the authors showed that any deviation in particle form from a sphere leads to an increase in the strength of the granular material. Preliminary results presented in [20] showed that increases in strength are more sensitive to increases in particle elongation than particle platyness.

In this paper we focus on the effect that particle platyness has on the strength of a granular material at critical state. To isolate this effect, in the analyses reported here elongation was kept constant by setting $L = I$ and therefore $\zeta = 0$. Platyness on the other hand was varied by decreasing S between $S = 1$ (for $L = I = S$, a sphere) and $S = 0$ ($L = I$ and $S = 0$, a circular disk). The particle forms considered have dimensions $L = I \geq S$; a summary is given in Table 1.

Form	L : I : S	Platyness α	Elongation ζ
1	1 : 1 : 1	0	0
2	1 : 1 : 0.8	0.14	0
3	1 : 1 : 0.73	0.2	0
4	1 : 1 : 0.6	0.3	0
5	1 : 1 : 0.5	0.4	0
6	1 : 1 : 0.3	0.6	0

Table 1: Table of particle forms considered in the analyses reported here.

3 DEM Modelling

As physical tests on a granular material of a single particle form are very difficult to carry out, the Distinct Element Method (DEM) is used here to simulate triaxial tests. DEM has been used extensively in the field of soil mechanics due to its ability to provide micro-mechanical information on the material at the particle scale. For this paper an in house DEM code was used, detailed in [14], that can accommodate smooth, convex particles of arbitrary shape. Hertzian interparticle contact is assumed.

Models were created using particles of a single form and a particle size distribution

(PSD) representative of that of railway ballast. They were then used to simulate triaxial compression conditions. To determine the PSD, 5 different sizes between the maximum and minimum gradation curves for railway ballast as defined in [1] were created for each model, keeping I equal to the respective sieve size.

To help constrain the models and ensure comparability of results, the total volume contained within each model was kept as close to $0.2m^3$ as possible. As a result the number of grains contained within each model varied with particle shape, however this is also the case with specimens of fixed dimensions used in physical tests.

To create a model, a number of particles were randomly dispersed within 3D space to a target initial void ratio of 2.0. The particles themselves were given random orientation to remove any bias in the initial conditions that could affect results.

The model was then subjected to isotropic compression using periodic boundaries, zero gravity forces and zero inter-particle friction. Once a void ratio of 0.65 was reached, isotropic stress of $100kPa$ was applied to the boundaries and the model was allowed to reach equilibrium. At that point inter-particle friction was reintroduced and the model was subjected to triaxial loading, where the lateral boundaries were stress controlled at a constant $100kPa$. The top boundary was strain controlled and moved downwards at a constant axial strain rate.

Table 2 shows the different model parameters that where used.

Properties	Value
Particle Density	2700Kg/m^3
Interparticle Friction Angle	30 degrees
Particle Bulk Modulus	50 GPa
Particle Poison's Ratio	0.3

Table 2: Material Properties

4 Results

4.1 Shear Strength

Mobilisation of shear strength of a granular material can be described by the mobilised angle of friction ϕ_{mob}, given by Equation 2.

$$\phi_{mob} = \sin^{-1}\left(\frac{\sigma_1 - \sigma_2}{\sigma_1 + \sigma_2}\right) \tag{2}$$

where σ_1 and $\sigma_2 = \sigma_3$ are the principal stresses. Figure 2 plots the mobilised angle of friction against vertical strain for each model. Whilst peak friction angles differ widely, these are not directly comparable because they may correspond to different initial relative densities of the granular materials modelled. (Although it could be argued that, due to the preparation procedure, all models were prepared at or near the densest state possible for

each material and therefore at or near unit relative density, this discussion is reserved for a future publication.) Due to the presumed difference in relative density among models, some reach a very dense packing that results to an almost immediate mobilisation of a very high angle of friction. Other models exhibit a delayed mobilisation of a rather lower peak.

The difference in relative density arises because varying the shape of the particles varies the minimum and maximum achievable void ratio. Therefore, even if two models are sheared from the same initial void ratio, their initial relative densities will most likely differ, precluding meaningful comparisons of peak friction. We note that theoretical estimation of the minimum and maximum void ratios is very difficult; research in the field of particle packing of different shapes does exist, however this is currently limited to mono-dispersed particles [15, 10].

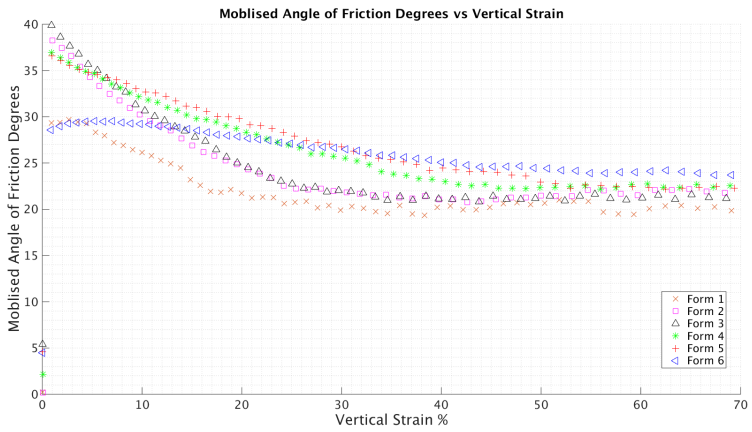

Figure 2: Mobilised angle of Friction against Vertical strain

On the other hand, the friction angle at critical state ϕ'_{crit} is independent of the initial void ratio, allowing valid comparisons. Figure 3 shows that as the shape of the particles becomes more platy, critical state strength increases roughly linearly with platyness.

4.2 Particle Orientation Fabric

At the start of the test, particles have a random orientation. However, as shearing takes place, particles will generally reorient themselves and may do so along some preferred direction. The orientation of each (ellipsoidal) particle can be described by a local system of orthogonal vectors in the directions of its three radii (L, I and S.) The average particle orientation with respect to the global model axes can be quantified by a fabric tensor such as that given by Equation (3) [19]. This describes the average orientation of a set of n unit vectors V^k. For randomly oriented vectors the diagonal of G_{ij} will be equal to $\frac{1}{3}$ and off-diagonal values will be zero, indicating lack of a preferential direction.

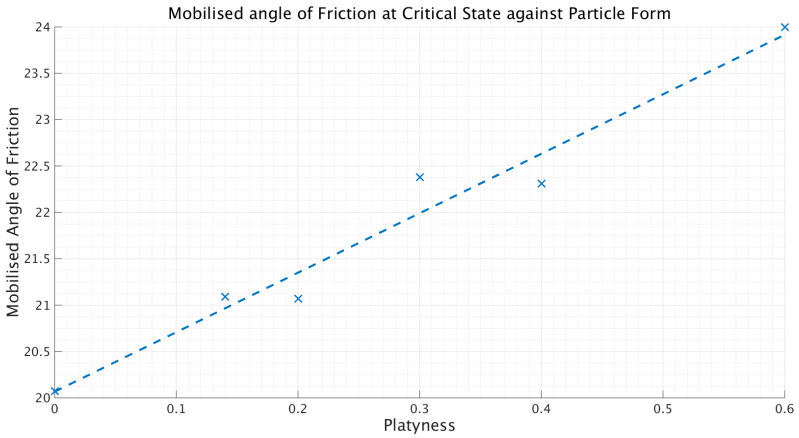

Figure 3: Friction angle at critical state against Platyness

$$G_{ij} = \frac{1}{n}\sum_{k=1}^{n} V_i^k V_j^k \tag{3}$$

As there is no single vector that describes the orientation of an ellipsoid, this fabric tensor can be calculated for the direction of each one of the three radii. Figure 4 shows how the G_{33} component of the fabric tensor corresponding to the S-direction of each particle varies with vertical strain. G_{33} essentially quantifies the prevalence of particles choosing to reorient their S-axis parallel to the global z-axis, i.e. with their flatter face normal to the maximum principal stress.

All tests started off with random particle orientation, shown by a value of $G_{33} \approx 0.33$ in Figure 4. As shear strains increased, however, so did G_{33}, showing that on average particles re-oriented their flatter face normal to the maximum principal stress in the course of shearing. Also, the rate of reorientation progressively decreases as the model approaches critical state, presumably because a configuration that can accommodate further shearing is reached. This general behaviour is observed even for relatively small values of platyness. In contrast, spherical particles do not show any tendency to re-orient and $G_{33} \approx const.$ throughout.

4.3 Particle Rotation and Sliding

As a specimen is strained, the particles will displace and rotate to accommodate this by rearranging the structure of the granular skeleton. It is expected that, during this process, particles of different forms will need to translate and rotate in different ways or proportions. Previous numerical studies of 2D assemblies have shown a link between particle rotations and sliding contacts; inhibiting rotation led to larger amounts of sliding and a higher mobilised angle of friction by increasing the amount of energy necessary to distort the skeleton [6].

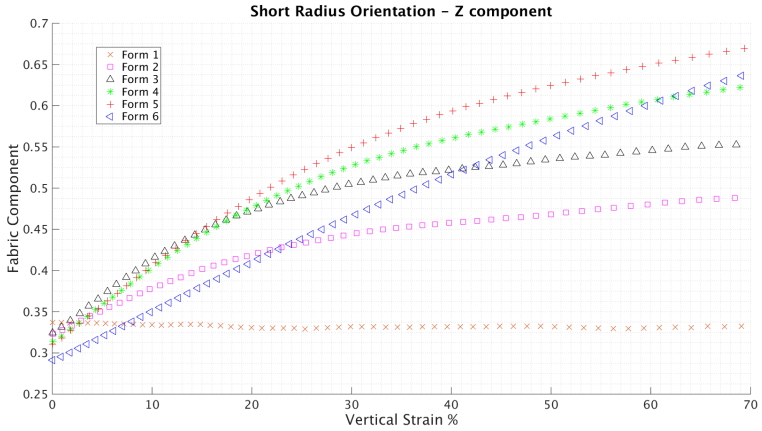

Figure 4: Vertical fabric orientation for the particle's S radius against Vertical Strain

Quantifying rotations and rotation increments in 3D in a meaningful way is more challenging, but can be simplified using the algebra of quaternions: rotation can be considered a quaternion whose real part quantifies the amount of rotation and its three imaginary parts the direction of the axis about which that rotation takes place. Here we focus on differences of the real part between relatively closely spaced time-steps, so that the axis of rotation can be considered unchanged, and divide rotation by the corresponding true vertical strain increment to produce a rate of rotation with strain given by Equation 4.

$$\theta = \frac{d\theta_{quat}}{d\epsilon_z} \tag{4}$$

Figure 5 plots the mean rate of particle rotation against the proportion of sliding contacts for the different particle forms at critical state. Spherical particles rotate much more compared to platy particles; the rate of rotation decreases with increased platyness. Also, as particle platyness increases there is a reduction in the proportion of sliding contacts at critical state. An inverse relationship is seen between rate of rotation and the proportion of sliding contacts at critical state. Therefore to some extent the higher critical state strength exhibited by platy particles is due to platyness suppressing particle rotation and leading to increased interparticle sliding, a mechanism that in comparison requires more energy to be expended.

4.4 Contact Distribution

Contact between two ellipsoids can be any one of six types, depending on which side of one ellipsoid comes into contact with which side of the other. Figure 6 shows the different types. The type of any given contact in a DEM simulation can be determined using the geometry of the contacting particles, the location of the contact point on their surfaces and geometrical arguments. For degenerate cases of ellipsoids, where some of the radii

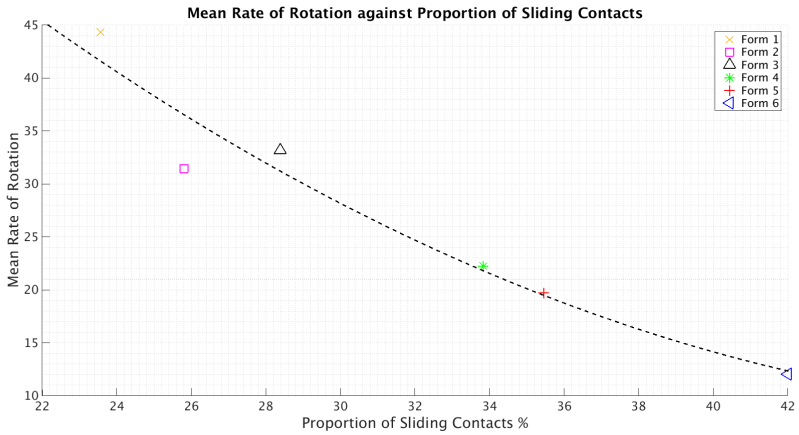

Figure 5: Mean proportion of sliding contacts against mean rate of rotation

are equal, the independent contact types are fewer: for example only one type of contact is possible between two spheres, where $L = I = S$.

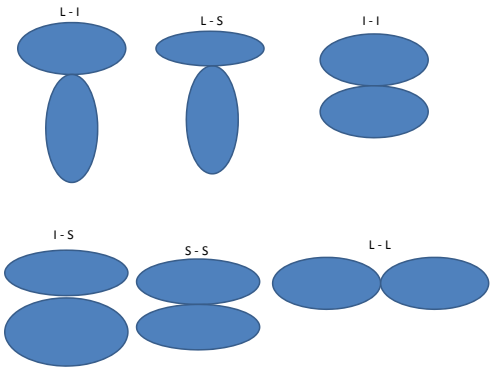

Figure 6: Different contact types for ellipsoidal particles

Figure 7 shows how the number of S-S ("flat-to-flat") as a percentage of the total number of contacts develops over time for each model. (For spherical particles the difference between L, I and S is simply operational and the data merely confirm that all "types" of contacts occur with the same probability as expected.) As the particle shape becomes platier the proportion of S-S type contacts increases, to some extent reflecting the increasing area of "flat" particle surfaces available for contact. However, although for near-spherical (Form-2) particles the proportion of S-S contacts remains relatively constant (i.e. oscillating around the same value between 10% and 50% strain), for the platier shapes of Form-3, but especially Forms-4, 5 and 6, S-S contacts become even more

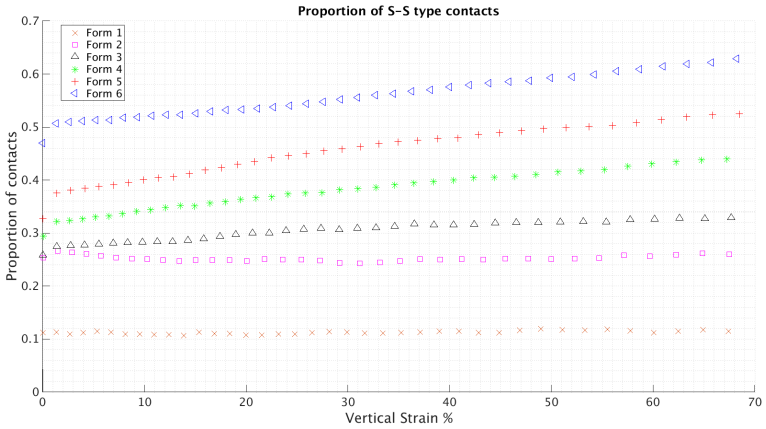

Figure 7: Distribution of contact type S-S against Vertical Strain

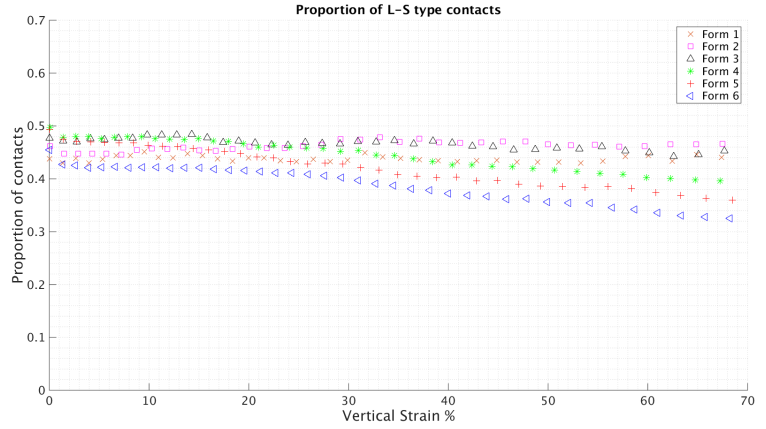

Figure 8: Distribution of contact type L-S against Vertical Strain

prevalent as the specimen is strained (e.g. varying by 7% over the same strain range for Form-6). This continuing formation of such contacts coincides with a more pronounced reorientation of particle flats normal to the maximum principal stress, as seen in Figure 4.

Figure 8 plots the proportion of L-S ("side-to-flat") contacts over time for all models. Similarly to S-S, it remains relatively constant for near-spherical particles (Form-2 but also 3.) In contrast to S-S, however, the proportion of L-S contacts for the platier particles (Form-4, 5 and 6) reduces with straining. The proportion of L-L ("side-to-side") type contacts, on the other hand, remains relatively constant throughout for all models; it is plotted in Figure 9.

The data suggest that, as the model is strained, platier particles promote a conversion of less stable L-S to inherently more robust S-S contacts that are less likely to subsequently break. Finally, there appears to be a threshold value $0.2 \leq \alpha_{cr} \leq 0.3$ of platyness, where a

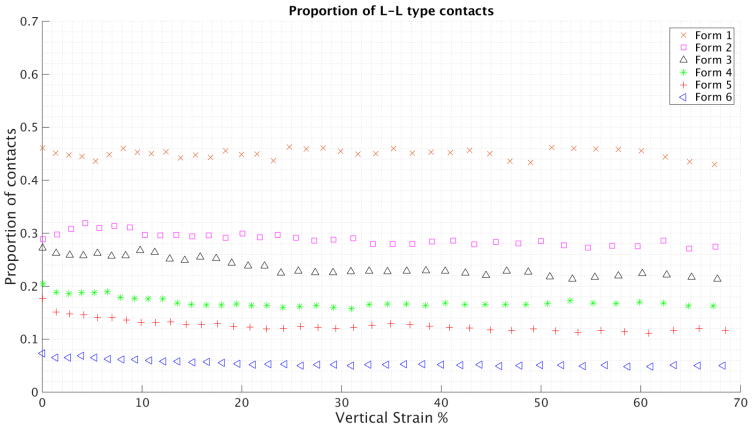

Figure 9: Distribution of contact type L-L against Vertical Strain

transition takes place to this type of "platy" behaviour for $\alpha \geq \alpha_{cr}$, from "near-spherical" behaviour for $\alpha \leq \alpha_{cr}$.

5 Conclusion

In this paper we used DEM to investigate the effect of particle platyness on granular material strength.

It was found that as particle platyness increases, so does the strength of the aggregate at critical state. This is accompanied, or rather is the result of, a reduction of particle rotation, which is inhibited by particle platyness, and a corresponding increase in the prevalence of interparticle sliding as the micro-mechanism that accommodates macroscopic straining.

Platier particles also showed a preference for aligning their flatter faces normal to the major principal stress and for forming "flat-to-flat" contacts, both of which arguably increase stability. A critical platyness value $0.2 \leq \alpha_{cr} \leq 0.3$ exists, governing the transition to "platy" behaviour, where more stable "flat-to-flat" contacts continue to develop during straining at the expense of other types, from "near-spherical" behaviour where this is not the case.

These observations are consistent with particle platyness promoting a more stable configuration of the granular skeleton, thus explaining the increased strength of the aggregate as measured macroscopically.

Acknowledgements

We gratefully acknowledge support from Network Rail (Strategic Partnership with the University of Southampton) and EPSRC Track21 Programme Grant, EP/H044949/1. Use of the IRIDIS High Performance Computing Facility and associated support services at Southampton are also acknowledged.

REFERENCES

[1] *BSI Standards Publication Aggregates for railway ballast BS EN 13450:2013 BSI*. BSI Standards Limited 2013, 2013.

[2] BC Aschenbrenner. A new method of expressing particle sphericity. *Journal of Sedimentary Research*, 1956.

[3] E Azéma and Farhang Radjaï. Stress-strain behavior and geometrical properties of packings of elongated particles. *Physical Review E*, 81(5):1–17, April 2010.

[4] E Azéma and Farhang Radjaï. Force chains and contact network topology in sheared packings of elongated particles. *Physical Review E*, 85(3):031303, March 2012.

[5] E Azéma, Farhang Radjaï, Baptiste Saint-Cyr, Jean-Yves Delenne, and Philippe Sornay. Rheology of three-dimensional packings of aggregates: Microstructure and effects of nonconvexity. *Physical Review E*, 87(5):052205, May 2013.

[6] J.P. P Bardet. Observations on the effects of particle rotations on the failure of idealized granular materials. *Mechanics of Materials*, 18(2):159–182, July 1994.

[7] P J Barret. The shape of rock particle, a critical review. *Sedimentology*, 27:291–303, 1980.

[8] SJ Blott and K Pye. Particle shape: a review and new methods of characterization and classification. *Sedimentology*, pages 31–63, September 2007.

[9] Bernard Cambou, Michel Jean, and Farhang Radjaï. *Micromechanics of granular materials*, volume 77. John Wiley & Sons, 2010.

[10] A Donev, FH Stillinger, PM Chaikin, and S Torquato. Unusually dense crystal packings of ellipsoids. *Physical review letters*, 2004.

[11] Nicolas Estrada, E Azéma, Farhang Radjaï, and Alfredo Taboada. Identification of rolling resistance as a shape parameter in sheared granular media. 011306:1–5, May 2011.

[12] Nicolas Estrada, Alfredo Taboada, Farhang Radjaï, Masami Nakagawa, and Stefan Luding. Shear strength and fabric properties in granular media with interlocked particles. *AIP Conference Proceedings*, 1145(2009):373–376, June 2009.

[13] Robert L. Folk. Student Operator Error in Determination of Roundness, Sphericity, and Grain size. *Journal of Sedimentary Research*, 25(4), 1955.

[14] J Harkness. Potential particles for the modelling of interlocking media in three dimensions. *International Journal for Numerical Methods in Engineering*, 80:157315(June):1573–1594, 2009.

[15] S. Heitkam, W. Drenckhan, and J. Fröhlich. Packing Spheres Tightly: Influence of Mechanical Stability on Close-Packed Sphere Structures. *Physical Review Letters*, 108(14):148302, April 2012.

[16] JE Dobkins Jr and RL Folk. Shape development on Tahiti-nui. *Journal of Sedimentary Research*, 1970.

[17] William Christian Krumbein. Measurement and Geological Significance of Shape and Roundness of Sedimentary Particles. *SEPM Journal of Sedimentary Research*, Vol. 11(2):64–72, August 1941.

[18] Duc-Hanh Nguyen, E Azéma, Philippe Sornay, and Farhang Radjaï. Effects of shape and size polydispersity on strength properties of granular materials. *Physical Review E*, 91(3):032203, March 2015.

[19] Masanobu Oda. Initial fabrics and their relations to mechanical properties of granular material. *Soils and Foundations*, 12(1):17–36, February 1972.

[20] M Potticary, A Zervos, and J Harkness. A numerical investigation into the effect of particle form on the strength of granular materials. In *Proceedings of the 22nd UK Conference of the Association for Computational Mechanics in Engineering*, number April, 2014.

[21] Farhang Radjai and Emilien Azéma. Shear strength of granular materials, 2009.

[22] Farhang Radjaï, Stephane Roux, and Jean Jacques Moreau. Contact forces in a granular packing. *Chaos (Woodbury, N.Y.)*, 9(3):544–550, September 1999.

[23] ED Sneed and RL Folk. Pebbles in the lower Colorado River, Texas a study in particle morphogenesis. *The Journal of Geology*, 1958.

[24] Hakon Wadell. Volume, Shape, and Roundness of Rock Particles. *The Journal of Geology*, Vol. 40(No. 5 (Jul. - Aug., 1932)):pp. 443–451, 1932.

[25] CK Wentworth. The shape of beach pebbles, 1922.

[26] EM Williams. A Method of Indicating Pebble Shape with One Parameter: NOTES. *Journal of Sedimentary Research*, 1965.

[27] Theodor Zingg. *Beitrag zur Schotteranalyse*. PhD thesis, 1935.